Journal of Quantitative Spectroscopy & Radiative Transfer 130 (2013) 260–272

Contents lists available at ScienceDirect

Journal of Quantitative Spectroscopy & Radiative Transfer

journal homepage: www.elsevier.com/locate/jqsrt

Re-analysis of ammonia spectra: Updating the HITRAN $^{14}NH_3$ database

Michael J. Down [a], Christian Hill [a], Sergei N. Yurchenko [a], Jonathan Tennyson [a,*], Linda R. Brown [b], Isabelle Kleiner [c]

[a] Department of Physics and Astronomy, University College London, London WC1E 6BT, UK
[b] Jet Propulsion Laboratory, M/S 183-601, 4800, Oak Grove Drive, Pasadena, CA 91109, United States
[c] Laboratoire Interuniversitaire des Systèmes Atmosphériques, UMR CNRS 7583, LISA, F-94010 Creteil, France

ARTICLE INFO

Article history:
Received 10 January 2013
Received in revised form
16 May 2013
Accepted 23 May 2013
Available online 7 June 2013

Keywords:
Ammonia
Line assignments
Atmospheric physics
Planetary atmospheres

ABSTRACT

The data incorporated in the HITRAN database for $^{14}NH_3$ are analyzed using a comprehensive and consistent set of quantum numbers, empirical lower energy levels and the BYTe variationally calculated line list as reference points. Labelings are checked to ensure that they obey both the usual selection rules and the HITRAN labeling formalisms; the problems identified are corrected where possible. Further assignments are brought into question by combination difference (CD) checking of implied upper energy levels. The CD analysis yields an 89% complete $^{14}NH_3$ energy level list up to 6610 cm^{-1} and $J=21$, self-consistent to 0.1 cm^{-1}. In combination with the 1723 previously unassigned and unlabeled lines in HITRAN a total of 2529 problem lines were identified for re-analysis. The compiled energy level list was used to label and assign the set of problem transitions, resulting in a total of 249 new assignments and a further 368 new labelings. Assignment by comparison with the reference line list resulted in 111 further new line assignments and 14 new labelings. Intensities are checked against recent measurements and BYTe. New intensities are proposed for the ν_2 band with new intensities and line positions for the $2\nu_2-\nu_2$ and new line lists are created for the $\nu_2-\nu_2$, $\nu_2-\nu_4$ and $\nu_4-\nu_4$ bands. BYTe band intensities are analyzed to identify other regions of missing intensity.

1. Introduction

Global ammonia emissions have more than doubled during the period of industrialization, largely due to widespread use of intensive agricultural techniques and in particular the use of fertilizers [1]. Furthermore, livestock, waste management, biomass burning and industry give additional anthropogenic contributions beyond that of nitrogen-based fertilizers. There are also a number of natural sources of ammonia including oceans, animal respiration and soil microbial processes which contribute to the global ammonia budget.

The release of ammonia into the atmosphere has a number of undesirable consequences, (e.g. Sutton et al. [2]) and there is a particular concern that the increasing presence of reactive nitrogen in our atmosphere, which comes from the release of ammonia, will lead to significant climatic consequences [3]. However, the actual ammonia emission budget remains uncertain, perhaps by up to 50% [4]. In particular its relatively short atmospheric lifetime and the large variability in its emissions means that any attempt to monitor ammonia concentrations should use high spatial resolution.

There have been a number of attempts to use spectroscopy to monitor atmospheric ammonia concentrations

* Corresponding author. Tel.: +44 20 7679 7809.
E-mail address: j.tennyson@ucl.ac.uk (J. Tennyson).

0022-4073
http://dx.doi.org/10.1016/j.jqsrt.2013.05.027

from space, such as the measurements reported from the IASI/MetOp [5], MIPAS [6] and TES [7] satellite experiments. These remote sensing applications are heavily dependent on the availability of reliable laboratory data for ammonia. However, the available laboratory spectroscopic data are not entirely satisfactory. For example, a very recent intercomparison of eleven ammonia measurement techniques [8] identified the quality of gas phase standards as one of the three significant issues affecting the precision of the measurements.

Ammonia is also known to be present in both gas giants [9] and cool brown dwarfs [10,11] where it provides an important source of opacity. Its presence has also been predicted in exoplanets [12,13], but is yet to be detected.

The room temperature spectroscopy of ammonia is encapsulated in the HIgh resolution TRANsmission molecular absorption database (HITRAN) [14]. Recent editions of this database incorporate 29 084 predominantly experimental transition frequencies and intensities for two isotopologues. In most case labelings are also given using the normal mode convention for vibrational states and the usual rigid-rotor convention for rotational states. These data come from the 10 sources [15–24]. However, some of the data in HITRAN has not changed since the 1986 edition and recent experimental [25–29] and theoretical studies of the spectrum of ammonia [30–34] suggest problems with this compilation. In particular, a number of new measurements [25–28] identified problems with line intensities in the ν_2 band of the HITRAN data and Chu et al. [29] report new accurate intensities for the $2\nu_2-\nu_2$ band which raise further issues.

Whilst usually considered of secondary importance to the positions and intensities, correct assignment of upper and lower energy levels to observed transitions is imperative in the previously mentioned applications due to the Boltzmann factor in the transition intensity expression [35]. Hence, complete and accurate assignment of energy levels to experimental spectra is vital. However, this is not found to be uniformly true in HITRAN, for which several assignment issues have been identified. To achieve the goal of improved assignment it is usual, although not strictly necessary, to adopt some approximate set of quantum numbers to label the energy levels in some systematic manner. We note that for ammonia this is problematic for higher polyads [23,36]. In this work we propose a consistent set of quantum numbers for the energy levels of ammonia and then attempt to use these for the transitions given in HITRAN. At the same time we compare the HITRAN line intensities with recent measured [25–28] and calculated [34,33] intensities and propose a number of improvements.

Throughout the analysis we make frequent use of the variational line list due to Yurchenko, Barber and Tennyson [34] henceforth referred to as BYTe. These calculations used an empirically refined potential energy surface [37], an *ab initio* dipole moment surface [38] and the program suite TROVE [39] for all nuclear motion calculations. TROVE uses a unique local mode representation and a truncated expansion for the kinetic energy operator. Labels, in either local modes or the ordinary normal mode quantum numbers, must be estimated via expansion of the wave-function. However, although such labels may be approximate in either convention, the calculations employ only rigorous quantum numbers and automatically account for all resonances. Experience has shown that use of empirically corrected frequencies with *ab initio* dipole moments is an effective method of predicting reliable transition intensities [40,41].

In this paper we review the current contents of the HITRAN database. The only lines we propose deleting from the HITRAN data are those 51 lines belonging to $2\nu_2-\nu_2$ we consider to be unreliable (see below). Section 8 describes the addition of many more new lines produced using a combination of empirical energy levels and BYTe intensities in the $2\nu_2-\nu_2$, $\nu_2+\nu_4-\nu_4$, $\nu_4-\nu_2$, $\nu_4-\nu_4$ and $2\nu_2-2\nu_2$ hot bands, which leads to a final line list with an increased total size of 40 224 lines.

2. Ammonia quantum numbers

As nicely illustrated by Fig. 69 in Herzberg [42], the structure of quantum numbers of ammonia energy levels becomes increasingly complicated upon multiple excitation of the degenerate modes. This leads to the problem of under specified states when using the traditional quantum numbers employed by HITRAN, in regions involving multiple excitations of degenerate vibrations.

To counter this problem, we suggest the following 13 quantum labels as a complete set describing the vibration–rotation states of the non-rigid NH_3 molecule:

$$\upsilon_1,\upsilon_2,\upsilon_3,L_3,\upsilon_4,L_4,L,\Gamma_{\rm vib},J,K,i,\Gamma_{\rm rot},\Gamma_{\rm tot}, \quad (1)$$

where $L_3=|l_3|$, $L_4=|l_4|$, $L=|l|$, $K=|k|$. Here υ_i, $(i=1,2,3,4)$ are the vibrational normal mode quantum numbers, l_3, l_4, and l are the vibrational angular momentum labels; J is the total angular momentum quantum number, $k=-J,\ldots,J$ is the projection of the total angular momentum on the molecule fixed axis z; $i=a/s$ is the inversion symmetry of the vibrational motion; and $\Gamma_{\rm vib}$, $\Gamma_{\rm rot}$ and $\Gamma_{\rm tot}$ are the symmetry species of the rotational, vibrational, and total internal wave-functions in the molecular symmetry group $\mathcal{D}_{3h}$(M) [35], respectively, spanning A'_1, A''_1, A'_2, A''_2, E', and E''. Since we only consider the ground electronic state, which for ammonia is a singlet state, we use $\Gamma_{\rm tot}$, which is equivalent to $\Gamma_{\rm rve}$, the symmetry species of the total internal wave-function excluding nuclear spin. Because of the nuclear spin statistics of ammonia, $\Gamma_{\rm tot}\neq A'_1,A''_1$. Use of the symmetry labels $\Gamma_{\rm tot}$ and $\Gamma_{\rm vib}$, in theory allows us to omit the commonly used inversion labels $(+/-)$ or s/a (see below). However, these are retained as a useful tool in spectroscopic analysis. These 13 quantum numbers are sufficient to completely describe the behavior of the four normal modes of vibration, two of which are doubly degenerate, and the rotation and inversion of the molecule. However, not all of them are always necessary, i.e. for many low-lying states this quantum number set is over-specified.

As ammonia's ground electronic state is a singlet state possessing no total electronic orbital angular momentum $J=N$, where N is the rotational angular momentum. The rotational assignment is usually associated with the rigid rotor wave-functions $|J,k,m\rangle$, where $m=-J,\ldots,J$ is the

Table 1
Symmetry species of the rotational states of ammonia in the $\mathcal{D}_{3h}$(M) group ($n=0,1,2\ldots$ and $K\geq 0$) [35].

K		Γ_{rot}
0	J even	A'_1
	J odd	A'_2
$6n\pm1$		E''
$6n\pm2$		E'
$6n+3$		$A''_1+A''_2$
$6n+6$		$A'_1+A'_2$

projection of the total angular momentum on the laboratory fixed axis Z. For reasons explained below we describe rotation using the absolute value of k, $K=|k|$ (see Eq. (1)). When symmetrized (see Ref. [43]) the rigid rotor functions can also be associated with the irreducible representation of $\mathcal{D}_{3h}$(M), as described in Table 1. The permutation (23) can be used to distinguish the $A_1^\dagger$ and $A_2^\dagger$ ($\dagger='$ and $''$) components in Table 1, see, for example, Ref. [43]. This operation leaves the $A_1^\dagger$ function unchanged, while acting (23) on the $A_2^\dagger$ rotational function changes its sign. This is usually associated with the rotational parity $s=(-1)^{\tau_{rot}}$, where $\tau_{rot}=0,1$ [43].

The Herzberg convention assigns the symmetric stretching mode ν_1 and symmetric bending mode ν_2 (often referred to as the umbrella or inversion motion) with the quantum numbers v_1 and v_2 respectively, which are usually associated with the one-dimensional (1D) harmonic oscillator wavefunctions [35]. The inversional umbrella motion (ν_2) is responsible for observable tunneling splitting between the two equivalent equilibrium structures, which split every energy level into a doublet. This gives rise to the commonly used inversion labels, $i=s/a$ for the umbrella mode ν_2^i, sometimes denoted $\nu_2^\pm$, which determine whether a given state is symmetric or antisymmetric on inversion through the planar configuration, respectively. The two doubly degenerate vibrational motions ν_3 and ν_4 are assigned v_3 and v_4 respectively and give rise to the additional vibrational angular momentum labels l_3 and l_4, where $l_i=-v_i,-v_i+2,\ldots,v_i-2,v_i$ with i=3,4. This description is usually linked to the 2D isotropic harmonic oscillator wavefunctions $|v_i^{l_i}\rangle$ [35]. The vibrational angular momentum labels l_i can be associated with the symmetry of $|v_i^{l_i}\rangle$ as follows: l_i=0 corresponds to A'_1, $l_i=\pm 3n$ to A'_1 and A'_2 with $n=1,2,\ldots$ and $l_i\neq\pm 3n$ to E' for $n=0,1,2,\ldots$. The two vibrational angular momentum labels are then coupled into the total vibrational angular momentum $l=l_3+l_4$, which is also related to the distinct irreducible representation Γ_{vib} according to the rule given above, with one important exception: the l=0 wave-functions can span both A'_1 and A'_2. The role of label l is to assist in assignment of the total rovibrational state considering the coupling of the vibrational and rotational components. Towards this end the combination $G=k-l$ or $G=k+l$ (introduced by Hougen [44]) is often used in place of the total symmetry Γ_{tot}. G is a good quantum number [44] for a XY_3 molecule even though neither l nor k are. This gives rise to the following set of quantum numbers commonly used in different combinations (compare to Eq. (1)):

$$v_1,v_2,v_3,l_3,v_4,l_4,l,i,J,k,G, \tag{2}$$

which in principle should be sufficient to unambiguously identify any rovibrational state. However, in practice the signs of the projections of the angular momenta (both rotational and vibrational) are not always known; only their absolute values are physically meaningful [45–47]. Therefore, we propose instead using the labels $L_3=|l_3|$, $L_4=|l_4|$, $L=|l|$, and $K=|k|$ specifying the absolute values of the momenta projections. Similar labels have been adopted for an effective Hamiltonian study of methane [48]. In order to provide the missing information and resolve the splittings which arise from interaction of the vibrational and rotational states, we will require the vibrational and total symmetry labels Γ_{vib} and total Γ_{tot} in place of $i=s/a$ and $G=k-l$. The idea is to form the rovibrational assignment (1) starting from coupling the vibrational modes followed by their coupling with the rotational state with the help of the multiplication rules for $\mathcal{D}_{3h}$(M) [35]. This effectively leads to a manifold $(v_1,v_2,v_3^{L_3},v_4^{L_4},L,J,K)$ spanning different values of Γ_{vib}, Γ_{rot} and Γ_{tot} as shown below.

The ν_1 mode has A'_1 symmetry and does not alter Γ_{vib} and Γ_{tot}. The coupling of ν_2, ν_3 and ν_4 will therefore define the vibrational symmetry labels in the molecular symmetry group $\mathcal{D}_{3h}$(M), including the labels $\dagger='(s)$ or $''(a)$ originating from the inversion parity (s/a) of the umbrella mode ν_2. This is due to the fact that the umbrella mode ν_2 has symmetry A'_1/A''_2 for (s/a) respectively.

In order to couple the $\nu_3^{L_3}$ and $\nu_4^{L_4}$ modes we use (i) the standard multiplication rules for irreducible representations and (ii) the rule for adding the angular momenta projections $l=l_3+l_4$. The latter in terms of the absolute values gives rise to two possible values for $L=|l|$ namely $L=L_3+L_4$ and $L=|L_3-L_4|$. The total vibrational symmetry Γ_{vib} is constructed as a product of the symmetry of the individual vibrational modes and the umbrella mode ν_2. The total symmetry Γ_{tot} is the product of the vibrational symmetry $\Gamma_{vib}=A'_1,A'_2,E',A''_1,A''_2,E''$ with the rotational symmetry spanning analogous irreducible representations of $\mathcal{D}_{3h}$(M) (see Table 1).

Let us consider an example of constructing all rovibrational states labeled $\nu_3+\nu_4$ ($v_1=0$, $v_2^i=0^s$ and $v_3=v_4=1$), and K=2. In the representation of Eq. (2) we obtain eight components corresponding to the following five states:

J	i	k	G	v_1	v_2^i	v_3	v_4	l_3	l_4	l
	s	−2	0	0	0^s	1	1	−1	−1	−2
	s	2	0					1	1	2
	s	±2	±4					∓1	∓1	∓2
	s	±2	∓2					∓1	±1	0
	s	±2	∓2					±1	∓1	0

The same five states in the representation of Eq. (1) read:

J	Γ_{tot}	K	Γ_{rot}	v_1	v_2	v_3	v_4	$\lvert l_3\rvert$	$\lvert l_4\rvert$	$\lvert l\rvert$	Γ_{vib}
	A'_1	2	E'	0	0	1	1	1	1	2	E'
	A'_2									2	E'
	E'									2	E'
	E'									0	A'_1
	E'									0	A'_2

The vibrational and rotational symmetry can be partly deduced, respectively, from the values of L and K. For

example the vibrational (rotational) state with $L(K)\neq 3n$ corresponds to the E irreducible representation. In this case the symmetry label $\Gamma_{\rm vib}$ ($\Gamma_{\rm rot}$) in Eq. (1) can be considered redundant. However, when $L(K)=3n$ an additional label is required to distinguish the two corresponding $A_1^{\dagger}$ and $A_2^{\dagger}$ components, for which $\Gamma_{\rm vib}$ and $\Gamma_{\rm rot}$ are used here. Alternatively, the parity label s could be used if following the labeling scheme suggested by Watson for X_3 molecules [49]. This label specifies the transformational property of the vibrational or rotational components of the function upon the permutation operation (23) (see above). Other schemes have also been proposed [50,51] for similar systems.

It should be noted that the number of vibrational states increases rapidly with multiple quanta of vibrational excitation. This leads to the situation that assignment of the approximate quantum numbers L_3, L_4, L, K is not always possible, due to mixing between wave-functions in the eigenfunctions, and simple counting quantum numbers have been used instead [20,23,36]. It is often the case [17,20,21,19] that upper states are strongly mixed and therefore not labeled with a full set of approximate quantum numbers. Transitions to such states are described as assigned but with upper states unlabeled.

The corresponding selection rules are the standard angular momentum selection rule, $\Delta J=0,\pm 1$ and the imposed symmetry conditions resulting from the general requirement,

$$\langle \phi'_{int}|\mu_A|\phi''_{int}\rangle\neq 0,\quad A=X,Y,Z, \tag{3}$$

where ϕ_{int} is a rovibration–inversion eigenfunction. These rigorous selection rules are given by parity change of the total internal wave function in any transition, and *ortho*/*para* conservation which stipulates for ammonia that the rovibronic-inversion symmetry species can only change between A'_2 and A''_2 for *ortho* nuclear spin states and E' and E'' for *para* nuclear spin states. The corresponding statistical weights $g_{\rm ns}$ are 12 for *ortho* (A'_2/A''_2) and 6 for *para* (E'/E'') states. The A'_1 and A''_1 states have $g_{\rm ns}=0$ since the corresponding nuclear spin states do not exist for a pyramidal XH_3 molecules of $\mathcal{D}_{3h}$(M) symmetry [35]. These rigorous selection rules are often expressed in terms of the good quantum number G as $\Delta G=\Delta(k-l)=0,\pm 3,\pm 6\ldots$, involving the non-rigorous quantum numbers k and l, with the additional propensity rule that $\Delta G=0$ transitions are "allowed" and those with $\Delta G\neq 0$ are "forbidden" and thus weak. In fact all HITRAN lines and all new assignments were required to meet these conditions in our updated version.

3. HITRAN problems

The starting point for present analysis is the 27 994 $^{14}NH_3$ transitions given in the 2008 edition of HITRAN [14] which in practice has not been updated since the 2000 HITRAN edition [52]. Table 2 lists the sources of the transitions given in HITRAN. The 1090 transitions of the $^{15}NH_3$ isotopologue are not considered here.

A first issue is that HITRAN only gives a maximum of nine quantum number labels: $\upsilon_1,\upsilon_2,\upsilon_3,\upsilon_4,l,i,J,K$ and in a few cases $\Gamma_{\rm vib}$. This specification is insufficient to describe ammonia's energy level structure in both the case where both l_3 and l_4 are non-zero, such as $\upsilon_3=\upsilon_4=1$ vibrational levels, and combinations where both the rotational and vibrational wave-functions have E symmetry which arise when $K=1,2,4,5,7,8,\ldots$ and $L=1,2,4,5,7,8,\ldots$.

Table 2
Summary of $^{14}NH_3$ data sources in HITRAN 2008 [14].

Range (cm^{-1})	Bands	No. lines	Refs.
0–2140	ν_0/ν_2 pure rotation	14 221	[24]
0–1245	$\nu_2/2\nu_2-\nu_2$	1616	[15]
1170–2160	$3\nu_2-\nu_2/\nu_2+\nu_4-\nu_2$	1250	[21]
1250–2135	$2\nu_2/\nu_4$	3692	[20]
2150–3100	$3\nu_2/\nu_2+\nu_4$	1151	[18]
2200–2750	$4\nu_2-\nu_2/\nu_1-\nu_2/\nu_3-\nu_2$	676	[22]
2980–3635	$\nu_1/\nu_3/2\nu_4$	3348	[23]
4030–4710	$\nu_1+\nu_2/\nu_2+\nu_3$	1130	[17]
4790–5295	$\nu_1+\nu_4/\nu_3+\nu_4$	2000	[19]

HITRAN makes use of only a single signed $l=l_3+l_4$ value. This gives rise to problems in the $\nu_3+\nu_4$ band where the translation between these two systems is not well defined for $l=0$. States with $l=0$ have two symmetry levels, A'_1 and A'_2 respectively (see above). Furthermore HITRAN uses a $l=-1$, 0, +1 labeling for this band rather than
$l=-2$, 0, +2.

We now turn to the actual line data in HITRAN. First it was found that a total of 933 lines of $3\nu_2/\nu_2+\nu_4$ in the 2150–3100 cm^{-1} region taken from Kleiner et al. [18], and $\nu_3+\nu_4/\nu_1+\nu_4$ in the 4790–5295 cm^{-1} region taken from Brown and Margolis [19], had conflicting assignment of inversion symmetry labels. This label is over-specified in the format adopted by HITRAN and the problem occurs when the rotational and vibrational quantum labels carry conflicting inversion symmetry labels. However, through testing for *ortho–para* violation and swapping of a and s labels it was possible to correctly assign all but 15 of these transitions, these 15 lines were therefore marked as unassigned.

Consistency checking of the already assigned lines resulted in many lower state energies having discrepancies greater than 0.1 cm^{-1}. These were found to come with two distinct sets of matching lower energies in most cases. To resolve these inconsistencies the empirical lower energies of Chen et al. [53] were used to replace all assigned lower energies. These provide a self consistent set for J up to 20 and therefore were complemented with empirical $J=21$, 22 levels taken from HITRAN, which our analysis and comparison with the results of Yu et al. [54] suggest are reliable.

Subsequently, upper energy levels were derived as the sum of these lower levels and transition wave-numbers as part of combination differences (CD) checking of implied upper energy levels. This resulted in 1973 transitions associated with 403 upper levels having combination difference errors greater than 0.01 cm^{-1}. The problem levels described were predominantly found to belong to two distinct energy values coming from different vibrational

bands and, in many cases, were also found to involve data from hot vibrational bands.

In particular, upper energy levels produced from transitions within the $2\nu_2-\nu_2$ hot band using data which originally appeared in the 1986 edition of HITRAN [14] are in consistent disagreement with the corresponding levels characterized using the $2\nu_2$ band of Cottaz et al. [20].

All assigned transitions were found to obey simple angular momentum selection rules. However, inspection revealed seven transitions which were removed from the data set for inspection as they violated both *ortho–para* conservation and parity rules. These strictly forbidden transitions came predominantly from the $\nu_3+\nu_4/\nu_1+\nu_4$ bands work of Brown and Margolis [19]. Inspection revealed that these lines broke the selection rules on K and l for this band only by the sign of l. Alteration of l labels in these misassigned lines successfully corrected all but one of these errors, and after a further check the corrected lines were replaced into the list. The remaining line was found to have a forbidden A'_1 lower state labeling which could not easily be corrected and was removed from the analysis for later reassignment. A further five lines from the work of Brown and Margolis [19] were found to have forbidden $K>J$ labelings which could not be easily corrected, and so were removed for reassignment.

4. The energy level list

From further CD it was then possible to derive an energy level list which combined the previously described lower energy levels and averages of implied upper energy levels derived from CD where possible. This was done as part of CD checking of the data in which the averages and deviations of all energies which agreed within 0.1 cm^{-1} were produced.

The original fitted data of Kleiner et al. [23] were used to replace the transition frequencies in HITRAN, for values that did not agree with this source of data, in an attempt to remove disagreements for the ν_1, ν_3 and $2\nu_4$ bands. In particular six CD problems greater than 0.1 cm^{-1} were resolved.

At this point only 113 transitions involving 35 upper levels had disagreements greater than 0.1 cm^{-1} and these were found predominantly to come from disagreement between the $2\nu_2$ and $2\nu_2-\nu_2$ data. Whilst the $2\nu_2$ frequency data of Cottaz et al. [20] are accurate up to about 10^{-4} cm^{-1}, the $2\nu_2-\nu_2$ data [15] are quoted with accuracy greater than 1 cm^{-1}. Furthermore, the $2\nu_2-\nu_2$ data are only referenced to the HITRAN 1986 database [15] and it was not therefore verifiable by comparison with an original source. As a result upper energy levels were derived from the $2\nu_2$ band where possible, and $2\nu_2-\nu_2$ lines from HITRAN 1986 not consistent with these values to within 1 cm^{-1} were not used in the analysis below. However, upper levels belonging to only $2\nu_2-\nu_2$ transitions were retained at this point.

Since all other CD upper levels occurred in bunches, it was possible to resolve all remaining problems by a judicious choice from two distinct sets of energy levels in each case. In this way most of problems were resolved where the majority of transitions agreed well, by choosing the average energy of the "good" set as the energy level. This logic was applied to all the remaining combination differences to select an energy level, and in general amounted to favoring data from "cool" rather than "hot" bands. Again, all transitions causing upper state discrepancies were removed for further analysis.

This process left a list of 3629 energy levels with average deviations of 3.6×10^{-5} cm^{-1} for lower states and 7.7×10^{-4} cm^{-1} for upper states derived from CD. Note it is not possible to derive deviations for upper state energies which had only one or two corresponding

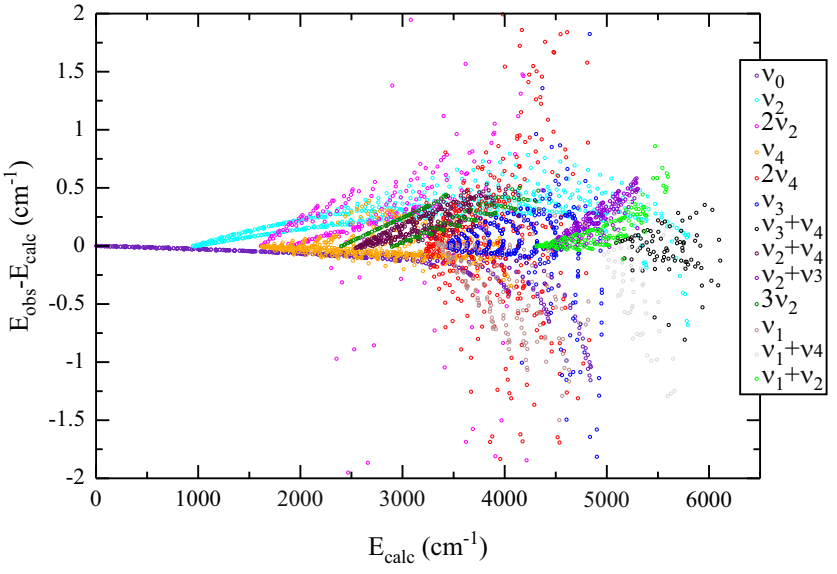

Fig. 1. Energy residuals between HITRAN derived empirical levels and variationally calculated BYTe levels following matching based on rigorous quantum numbers. Levels are color coded according to vibrational band. (For interpretation of the references to color in this figure caption, the reader is referred to the web version of this article.)

transitions but these are included in the energy list nevertheless for completeness. These observed energies were listed alongside the complete set of 4710 possible levels up to $J=21$ for the vibrational bands considered here. This constitutes an approximately 89% complete energy level set with a maximum energy at around 6100 cm^{-1}.

The energy levels were further verified by requiring a match with the BYTe energy levels based on the rigorous quantum numbers, total angular momentum J and total symmetry Γ_{tot}. The results of this matching are shown in Fig. 1 separated by vibrational band. At this point 26 $2\nu_2$ energy levels were removed, having no corresponding BYTe level within 10 cm^{-1}; these levels all have $J > 14$ and involve upper levels from the unreliable $2\nu_2-\nu_2$ band data. It is possible that the large residuals seen here between BYTe and corresponding HITRAN derived empirical energy values for some levels are due to errors in the variational calculations. However, this is thought to be unlikely for errors over 10 cm^{-1}, since such large errors are out of keeping with the residuals expected from inspection of Fig. 1. Such levels were hence deemed unreliable, and removed. This left 3603 levels.

Subsequently, the compiled energy levels were applied to the set of all remaining assigned transitions. In total 779 transitions were removed from the data set for re-analysis in this process as their assignments were considered dubious. In general the lower assignments of these transitions were still considered reliable. However, a question remains over the quality of the $2\nu_2-\nu_2$ transitions provided by HITRAN 1986 [15], and these lines are not analyzed further here. A remeasurement of the band is clearly necessary.

5. New assignments

Trivial assignments can be made when the difference between two energy levels which comprise an allowed transition is found to match the unassigned experimental frequency within its error margin. Ideally, a complete and sufficiently accurate energy level list combined with an accurate spectrum would allow all lines to be assigned in this way but this is not usually the case and other methods must be considered.

The complexity of the NH_3 spectrum has hindered the application of standard methods of assignment due to large inversion splitting, l-doubling, and the strong interactions between many different vibrational bands. We therefore employ methods which depend upon the knowledge of an accurate energy level list and/or calculated spectrum. It may be possible to assign transitions purely by comparison with a calculated line list. In order to avoid misassignments, previously assigned lines must be removed from the reference line list at this point. It is then possible to search for calculated lines with similar positions in the reference line list in order to make assignments. Furthermore, calculated transition intensities can be used to match lines in dense regions of the spectrum where the position alone is not enough to identify an assignment. This was found to be most successful when attempted graphically.

It is also possible to make use of the fact that errors between observed and calculated values within a vibrational band vary in a systematic way as J and K vary. This obs–calc error of any proposed assignments to already partially assigned branches of the spectrum may then indicate the validity of the assignments and the correct assignment can be more easily picked out. This technique known as the "method of branches" is explained further for water spectra by Polyansky et al. [55].

In comparison with calculated line lists, the break down of the normal mode model at higher energies adds an intrinsic flaw to attempting to assign vibrational quantum labels in the normal mode picture. Whilst many of the most accurate calculations are made using local mode theory in various coordinates, for comparison with experimental assignments the labels used are generally transformed into the traditional labels by some means: the largest coefficient of expansion method for example. However, this process is not perfect and may in some cases give rise to misleading vibrational labels. It is therefore important to remember that only the symmetry species, parity label and J quantum number of a state provide rigorous quantum labels and all other labels are approximate and in some cases arbitrary.

6. Assignments to HITRAN

Of the 1723 incompletely assigned $^{14}NH_3$ lines in HITRAN, 11 001 are unassigned lines in the 4790–5295 cm^{-1} region from Brown and Margolis [19] and 53 are unassigned lines in the 2200–2750 cm^{-1} region from Kleiner et al. [18]. The remaining 569 lines come from Cottaz et al. [20] in the 1335–1978 cm^{-1} region and Kleiner et al. [23] in the 3010–3598 cm^{-1} region with 249 and 421 lines respectively. These are partially assigned with lower state energies, complete lower labels and upper state J labels. This set was combined with the set of problem assignments prior to the assignment process. Note that in general the errors in the experimental frequencies are much larger than those in the lower-state energy levels (typically by three orders of magnitude) and so only this error was considered in what follows. Furthermore, selection rules were required to be obeyed by all new assignments.

Firstly, trivial assignments were attempted whilst retaining lower energy level assignments. This led to six labelings, all of which were labeled for the first time.

The remaining lines were recombined with the forbidden transitions prior to trivial assignment via our compiled energy level list. It was possible to trivially assign 128 lines to within the error of the HITRAN frequency, using

Table 3
Summary of assignments to HITRAN.

Type of assignment	No. assigned	New assigned	New labeled
Trivial labeling	6	0	7
CD labeling	485	0	260[a]
Trivial assignment	127	127	0
CD assignment	257	121	102
BYTe	162	111	14
Total	1038	360	378

[a] Upper state J labels were only altered for a small minority of lines.

the reference energy levels. All these were new assignments with new labelings.

CD labeling retaining HITRAN lower energies resulted in 250 new labelings and many confirming re-labelings. In this case upper energies were required to have a corresponding BYTe energy level match within a 1 cm^{-1} error, the matching levels only being permitted to have certain allowed J and Γ values. As a result 161 new levels were added to the compiled energy set.

Further CD resulted in 257 new assignments. Upper levels were required to agree better than five times the quoted experimental error in HITRAN, and only matches of at least three transitions or more corresponding to a single upper level were considered. Again upper energies were required to have a corresponding BYTe energy level match, from which the upper labels were taken. It is important to note that these labels may not always be exact, as will be discussed below. All the above assignments and labelings are summarized in Table 3.

A reference line list calculated variationally at 296 K using a rotation–contortion–vibration Hamiltonian with an intensity cut off at 1.7×10^{-39} cm^{-1}/(molecule cm^{-2}) at 296 K was produced using the BYTe line list.

To use BYTe to make assignments it is necessary first to remove the 26 266 verified lines already assigned in HITRAN from the BYTe line list in order to avoid duplicate assignments. However, the calculations used to construct BYTe use local mode theory and local mode labels. Normal mode labels must therefore be obtained using the largest coefficient approach and may not be exact. In particular the conversion process cannot distinguish properly between v_1 and v_3, whilst the sum $v_1 + v_3$ is always conserved. Furthermore only the magnitude of l_3 and l_4 labels in BYTe are reliable and so it is not always possible to derive the correct L label.

This makes direct matching of all transitions difficult and the problem is compounded by the large number of lines present in BYTe. However, by first matching the empirical energy levels with the BYTe calculated energy levels based on rigorous quantum numbers, and then calculating an equivalent BYTe frequency from lower and upper BYTe energies the problem is considerably simplified. The empirical energy levels were matched relatively easily to BYTe levels based on rigorous quantum numbers alone in most cases, due to the lower number of energy levels than transitions in the line list. The residuals shown in Fig. 1 show the systematic errors associated with the variational calculations made in BYTe.

In this way the vast majority of HITRAN lines (23 821) could be matched to a calculated BYTe transition and subsequently removed. At this point approximate intensity agreement was required, resulting in several hundred lines which could not be matched. Large intensity errors can be expected for weak lines due to larger experimental errors and difficulties in correctly modeling intensity stealing due to resonances in the variational calculations [56] such as BYTe. This can be seen in Figs. 2 and 3, which show the intensity agreement between BYTe and HITRAN lines plotted against line intensity and line position respectively.

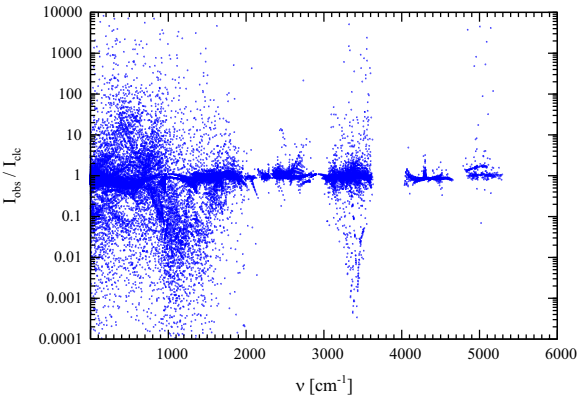

Fig. 3. Intensity ratios of HITRAN and variationally calculated BYTe values plotted against frequency of the transitions in question. Again, 5.0% of lines have intensity ratios $0.01 > I_{obs}/I_{calc} > 100$.

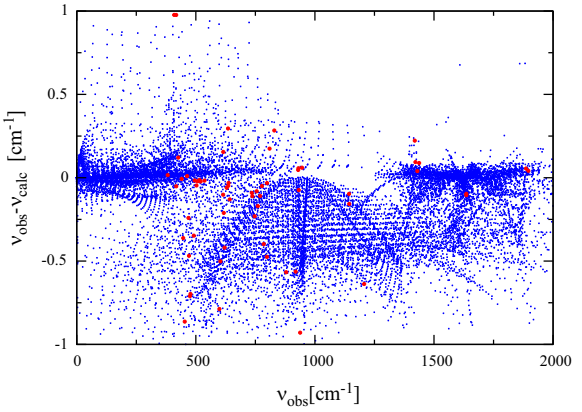

Fig. 4. Frequency residuals between HITRAN and variationally calculated BYTe levels. For clarity only a sample region (0–2000 cm^{-1}) is shown although behavior was similar elsewhere in the spectrum. New assignments (red) are shown on top of previous assignments (blue). (For interpretation of the references to color in this figure caption, the reader is referred to the web version of this article.)

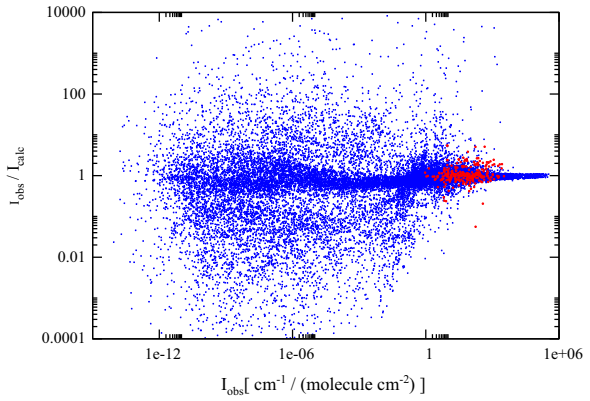

Fig. 2. Intensity ratios of HITRAN and variationally calculated BYTe values at 296 K. New assignments are shown on top of previous assignments in red. From all matched lines 5.0% have intensity ratios $0.01 > I_{obs}/I_{calc} > 100$. (For interpretation of the references to color in this figure caption, the reader is referred to the web version of this article.)

Among the matched lines, 5% have intensity ratios outside the range $0.01 < I_{obs}/I_{calc} < 100$. Of these, the majority can be seen in Fig. 2 to belong to weak lines for which we expect noisy intensity behavior. Such lines can also be seen in Fig. 3 to come largely from the microwave and far infrared transitions below 1500 cm^{-1} belonging to Refs. [15,24]. Intensities are discussed in greater detail in Section 7.

Following this removal, assignment of remaining HITRAN lines was attempted *via* direct comparison with BYTe, considering both positions and intensities. In doing so it was helpful to consider initially only the strongest intensities, and indeed little progress could be made with weaker lines. The results are summarized by Fig. 4 which shows the position residuals and Fig. 2 which shows the intensity ratios between BYTe and HITRAN for the new assignments. In both cases the assignments are shown alongside all previously verified HITRAN assignments. These results, again summarized in Table 3, included 107 assignments to previously unassigned lines, four reassignments and 15 new labelings. A further 36 assignments confirmed the HITRAN labelings and assignments. We emphasize that it is always possible that labelings derived from BYTe are not consistent with those from other sources. For a small number of lines vibrational labelings from HITRAN were altered to those from BYTe in cases of ambiguity. This resulted in a number of further new labelings some of which belong to vibrational bands new to HITRAN, which must therefore be considered somewhat tentative.

In total there were 133 tentative assignments to vibrational bands not present in the original HITRAN data. Such assignments include both new assignments and re-labelings of existing assignments using BYTe predicted energy levels where the HITRAN labelings are considered unreliable. These assignments are summarized in Table 4, the majority coming from the CD analysis. For the three assignments made by line list comparisons in the $4\nu_2-\nu_2$ band, two are in agreement with the 52 previous tentative assignments made in the $4\nu_2-\nu_2$ band by Cottaz et al. [21]. The remaining assignment is not verified by their work.

The 47 assignments made by the work of Huang et al. [32] to unassigned HITRAN data are also found by our work. These were in general agreement with our assignments although our BYTe derived labels differ in some cases. Out of these lines 18 (associated with five upper levels) required significant relaxation of the error margin used to achieve CD assignment. In some cases upper labels derived from BYTe also differed from Huang et al.'s labels in the manner previously discussed.

Table 4
Summary of $^{14}NH_3$ assignments to problem lines in HITRAN.

Problem	No. identified	No. assigned
Unassigned	1154	237
Unlabeled	569	457
Bad CD	779	339
Bad parity	15	4
Forbidden	7	0
$K > J$	5	1

Table 5
Summary of tentative assignments to HITRAN lines in new vibrational bands.

Band	No. assigned	J_{MIN}	J_{MAX}	No. levels
$2\nu_2+\nu_4$	66	5	19	28
$2\nu_2+2\nu_4$	27	4	13	10
$3\nu_4$	13	4	10	6
$\nu_1+2\nu_2$	12	6	11	4
$4\nu_2$	10	11	12	9
$2\nu_2+\nu_3$	7	7	10	2
$4\nu_2+\nu_4$	7	3	7	3
$4\nu_2-\nu_2$	3	3	6	9
$3\nu_2-\nu_2$	2	12	12	1
$\nu_1+\nu_2+\nu_4-\nu_2$	1	5	5	1

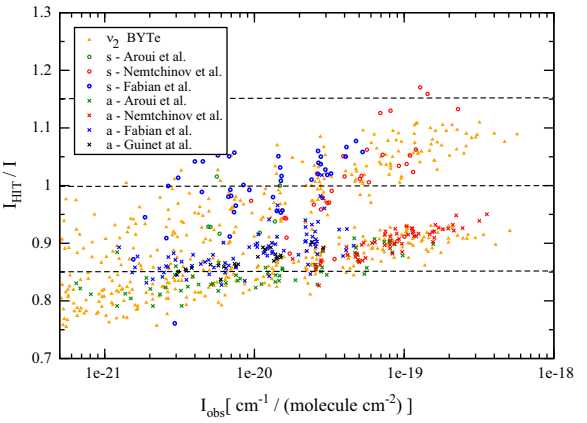

Fig. 5. Intensity ratios for the ν_2 band at 296 K: comparison of BYTe [34] and new measurements [25–28] with HITRAN [15]. Lines are grouped by symbol according to lower state symmetry (*a*/*s*). In general HITRAN intensities are found to be too weak for transitions from *a* symmetry lower levels. Dashed lines indicate upper and lower limits according to a HITRAN uncertainty estimate of 15%.

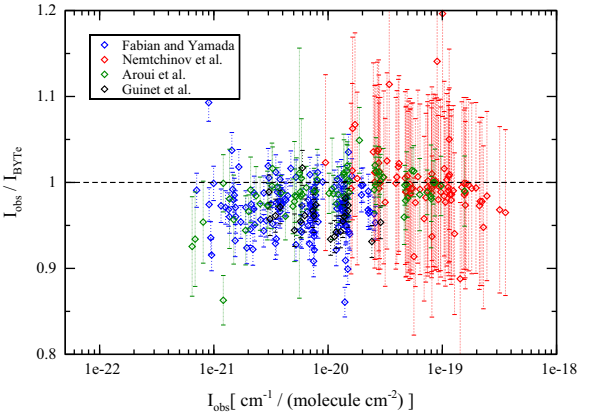

Fig. 6. Intensity ratios for the ν_2 band at 296 K: comparison of new experimental intensities from Refs. [25–28] with BYTe [34]. Error bars are taken from the experimental data where provided; for Nemtchinov et al. 10% error bars are used based on comparison with the other sources, since experimental uncertainties were not available. In each case the number of lines and root mean square deviation σ_{RMS} are shown in Table 6.

7. Intensity comparison

Comparisons of HITRAN intensities with BYTe and recent experimental values were carried out using quoted experimental errors and HITRAN error estimates. In general agreement was within these given errors, with three notable exceptions.

Firstly, the microwave and ν_2 far infrared data [24] were found to be very noisy for absolute intensities weaker than about 10^{-24} cm^{-1}/(molecule cm^{-2}) at 296 K. Furthermore, intensities from these sources were also systematically shifted, in some case by more than the estimated HITRAN uncertainty (15%) as seen in Fig. 5. The structure visible in general corresponds to transitions with a/s lower level inversion symmetry respectively, for the relatively weaker and stronger bunches of lines.

As further validation, ν_2 intensities were compared with the recent and more accurate experimental intensities available for the ν_2 band due to Fabian and Yamada [26], Guinet et al. [25], Nemtchinov et al. [27], and Aroui et al. [28]. These intensities show similar behavior and agree very well with BYTe as depicted in Fig. 6. The data are summarized in Table 6 alongside σ_{RMS} values of the BYTe comparison. Where possible, these intensities are used to replace the HITRAN values. Interestingly, the intensities of the small number of lines measured in this region very recently by Owen et al. [57] are in excellent agreement with both HITRAN and BYTe. Elsewhere, we use BYTe values for the ν_2 intensities which we consider more reliable than the HITRAN values in this band. However, we suggest the need for a comprehensive set of accurate experimental intensities in both this region and the microwave region as a priority.

Secondly, the intensity ratios of Brown and Margolis [19] when compared with BYTe were found to have structure, with many lines systematically about 40–50% too strong. However, these lines all came from the same vibrational band and we attribute this problem to the BYTe line list, in which errors may vary systematically between vibrational bands.

Table 6
Summary of recent intensity measurements for the ν_2 band of $^{14}NH_3$ [26,25,27,28], giving the number of lines, average deviation δ and root mean square deviation σ_{RMS} of comparison with BYTe [34] intensities.

Study	No. lines	Freq. range (cm^{-1})	J range	δ (%)	σ_{RMS} (%)
Guinet et al. [25]	22	1126–1172	9–11	−4.12	4.60
Nemtchinov et al. [27]	91	805–1118	0–8	−0.16	3.62
Fabian and Yamada [26]	126	770–1179	3–15	−3.05	4.82
Aroui et al. [28]	69	1067–1199	6–12	−1.29	3.03

Table 7
Vibrational band strengths derived from the updated HITRAN data set S^b compared with values derived from BYTe variational calculations S_{BYTe} and the previously published HITRAN data S_{HIT}. The values S^a are derived from previously published HITRAN data with BYTe intensities where possible. The number of transitions N contributing to each value is also shown. For BYTe this value includes all transitions in the 0–8000 cm^{-1} range with relative intensities greater than 10^{-12}. The band strengths are given at T=296 K in units of cm^{-1}/(molecule cm^{-2}) and do not include lines lacking vibrational assignment in HITRAN. Band origins are given in cm^{-1} and are taken from the relevant HITRAN sources [18–21,23] and for ν_2 the work of Chen et al. [53]. In each case values are for symmetric upper state transitions only.

Vib. band	Origin	S_{HIT}	N_{HIT}	S^a	N[a]	S^b	N[b]	S_{BYTe}	N_{BYTe}	S^a/S_{BYTe}
ν_0	–	1.72×10^{-17}	3888	1.76×10^{-17}	3668	1.72×10^{-17}	3891	1.76×10^{-17}	6187	0.977
ν_2	932.4	2.21×10^{-17}	6872	2.26×10^{-17}	6676	2.25×10^{-17}	6875	2.26×10^{-17}	12 193	0.992
$\nu_2-\nu_2$	–	1.42×10^{-19}	3409	1.55×10^{-19}	3300	1.41×10^{-19}	3409	1.55×10^{-19}	5604	0.910
$2\nu_2-\nu_2$	665.1	2.35×10^{-19}	655	1.78×10^{-19}	242	4.72×10^{-19}	2020	4.75×10^{-19}	11 321	0.993
$3\nu_2-\nu_2$	1963.1	1.39×10^{-20}	275	1.56×10^{-20}	275	1.39×10^{-20}	280	1.61×10^{-20}	10 909	0.865
$\nu_2+\nu_4-\nu_2$	1608.1	4.69×10^{-20}	975	4.75×10^{-20}	975	4.74×10^{-20}	986	4.88×10^{-20}	20 970	0.970
$2\nu_2$	1597.5	2.96×10^{-19}	882	2.91×10^{-19}	875	3.03×10^{-19}	924	3.13×10^{-19}	13 615	0.967
ν_4	1626.3	4.39×10^{-18}	2561	4.20×10^{-18}	2561	4.40×10^{-18}	2710	4.20×10^{-18}	25 265	1.049
$3\nu_2$	2384.1	1.79×10^{-20}	385	1.82×10^{-20}	332	1.77×10^{-20}	346	1.87×10^{-20}	11 646	0.943
$\nu_2+\nu_4$	2540.5	8.05×10^{-21}	975	6.72×10^{-21}	653	7.95×10^{-21}	986	7.34×10^{-21}	22 557	1.084
$\nu_3-\nu_2$	2511.2	5.07×10^{-21}	461	5.39×10^{-21}	461	5.07×10^{-21}	455	5.99×10^{-21}	24 481	0.847
ν_1	3336.1	8.53×10^{-19}	473	8.82×10^{-19}	473	8.63×10^{-19}	536	9.08×10^{-19}	15 212	0.950
ν_3	3343.6	4.50×10^{-19}	1031	4.97×10^{-19}	1029	4.51×10^{-19}	1042	5.01×10^{-19}	30 712	0.900
$2\nu_4$	3228.4	2.19×10^{-19}	1524	2.35×10^{-19}	1492	2.28×10^{-19}	1659	2.56×10^{-19}	30 701	0.890
$2\nu_4-\nu_2$	2298.9	2.43×10^{-22}	215	2.44×10^{-22}	215	2.57×10^{-22}	215	5.09×10^{-22}	25 811	0.505
$\nu_1+\nu_2$	4294.5	1.13×10^{-19}	385	8.24×10^{-21}	105	1.13×10^{-19}	384	1.34×10^{-19}	17 605	0.841
$\nu_2+\nu_3$	4416.9	6.51×10^{-19}	745	7.17×10^{-19}	506	7.33×10^{-19}	628	8.24×10^{-19}	31 758	0.890
$\nu_1+\nu_4$	4955.8	3.07×10^{-20}	234	8.24×10^{-21}	105	8.81×10^{-20}	253	6.73×10^{-19}	66 042	1.308
$\nu_3+\nu_4$	5052.6	6.36×10^{-19}	665	1.97×10^{-19}	208	3.68×10^{-19}	429	4.52×10^{-20}	29 610	0.814
$\nu_1+\nu_4/\nu_3+\nu_4$[c]	–	6.67×10^{-19}	899	2.05×10^{-19}	313	4.56×10^{-19}	682	7.19×10^{-19}	95 652	0.635
$\nu_4-\nu_4$	–	–	–	–	–	1.25×10^{-20}	2823	1.29×10^{-20}	17 671	0.967
$2\nu_2-2\nu_2$	–	–	–	–	–	1.75×10^{-20}	860	1.77×10^{-20}	5810	0.992
$\nu_4-\nu_2$	693.8	–	–	–	–	3.98×10^{-20}	3585	4.12×10^{-20}	19 455	0.966
$\nu_2+\nu_4-\nu_4$	914.3	–	–	–	–	1.78×10^{-20}	3600	1.82×10^{-20}	32 915	0.977

[a] Values derived using only lines in HITRAN with intensities taken from BYTe where possible. Note that for many bands lines with significant total intensity could not be matched with BYTe.
[b] Values derived from our updated HITRAN data set using the results of this work.
[c] Due to BYTes failure to consistently distinguish between υ_1 and υ_3 quanta the band strengths here are best compared in combination.

Table 8
BYTe predicted band strengths (10^{-20} cm^{-1}/(molecule cm^{-2})) and band origins (cm^{-1}) for bands not yet included in HITRAN but with predicted band strengths greater than 10^{-20} cm^{-1}/(molecule cm^{-2}). Band origins are derived from symmetric $J=0$ BYTe energy levels. For degenerate states the lowest energy states are chosen.

Vib. band	Origin (cm^{-1})	S_{BYTe}	N_{BYTe}
$\nu_1+\nu_3$	6608.5	17.93	30 348
$\nu_1+2\nu_4$	6603.7	11.85	76 115
$\nu_1+\nu_2+\nu_4$	5899.5	4.150	63 332
$\nu_4-\nu_2$	693.8	4.123	19 455
$2\nu_2+3\nu_4$	6310.3	3.328	26 237
$2\nu_3$	6793.1	3.289	83 570
$\nu_2+2\nu_4$	4115.6	3.060	30 141
$2\nu_2+\nu_3-\nu_2$	4213.8	1.994	28 943
$2\nu_2+\nu_4$	3189.0	1.974	21 768
$3\nu_2$	2384.2	1.872	11 646
$\nu_2+\nu_4-\nu_4$	914.3	1.817	32 915
$2\nu_2-2\nu_2$	–	1.768	5810
$\nu_1+2\nu_2+\nu_4$	6590.1	1.716	66 295
$3\nu_2-\nu_2$	1451.7	1.605	10 909
$\nu_2+\nu_3-\nu_2$	3484.5	1.478	24 498
$\nu_4-\nu_4$	–	1.290	17 671
$\nu_1+\nu_2+\nu_3$	7656.3	1.249	28 955
$3\nu_2-2\nu_2$	786.7	1.096	9852

Thirdly, consistent disagreement was found for the $2\nu_2-\nu_2$ hot band, which has uncertainty in HITRAN quoted as "unreported or unavailable". Where possible these intensities were compared with BYTe values and the 12 experimental values reported by Chu et al. [29]. These lines have I_{HIT}/I_{BYTe} values with a trend which tends to 0.5 at strong intensities. Comparison of HITRAN with the 10 Chu et al. lines which could be matched verifies this finding having a mean I_{HIT}/I_{Chu} value of 0.49. The intensities of this band are clearly of poor quality, and considering the poor quality of positions in this band mentioned earlier a new line list was produced as outlined in the following section.

Elsewhere, intensities were in satisfactory agreement although we note the conservative estimated uncertainties of HITRAN as a reason for further improvement.

Finally, as a measure of completeness, band strengths for each of the vibrational bands included in HITRAN were compared with BYTe calculations for both previous and updated HITRAN data sets. The values are compared in Table 7, alongside the number of transitions included in each summation. For BYTe the band strengths included all lines with relative intensity stronger than 1×10^{-12} times the strongest line (5.516×10^{-19} cm^{-1}/(molecule cm^{-2})), in the 0–8000 cm^{-1} range. It is important to note that since these band strengths depend on vibrational labeling, interacting bands and bands for which BYTe labeling is considered unreliable may be better treated as a combined summation.

It is easy to use Table 7 to determine the regions where HITRAN is lacking. In particular the $2\nu_2-\nu_2$ and $2\nu_4-\nu_2$ bands appear to lack significant intensity. Furthermore BYTe band strengths given in Table 8 indicate several bands carrying significant intensity not yet incorporated in HITRAN 2008. These include the $\nu_1+2\nu_4$, $\nu_1+\nu_3$ and $2\nu_3$ bands analyzed recently by Sung et al. [36] and Cacciani et al. [58] which are being made available in the new 2012 release of HITRAN [59].

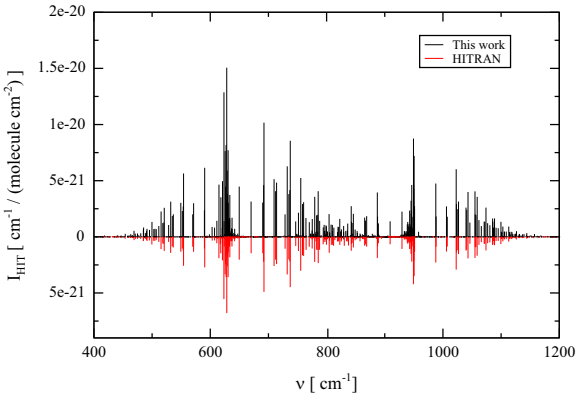

Fig. 7. Comparison of $2\nu_2-\nu_2$ lines for previous HITRAN data and the results of this work.

8. New line lists for hot bands

Due to the poor quality of positions and intensities in the $2\nu_2-\nu_2$ band described above, and the lack of line data for the $\nu_2+\nu_4-\nu_4$, $\nu_4-\nu_2$, $\nu_4-\nu_4$ and $2\nu_2-2\nu_2$ bands seen in Table 8, new line lists were created using the empirical energy levels previously derived from HITRAN, and BYTe intensities. The strategy of constructing reliable line lists using empirical energy levels and *ab initio* transition intensities has recently been extensively tested for water [56].

For the new line lists, BYTe lines stronger than the HITRAN intensity threshold described by Rothman et al. [60] were matched with new positions, computed from the empirical energy levels, where reliable upper and lower energy levels were available. The line lists were then formed from these new positions and lower energies alongside BYTe intensities and labelings. Due to a lack of upper levels this was not necessarily possible for all lines. The number of lines produced and the band strengths for the updated line lists are included in Table 7.

In the case of $2\nu_2-\nu_2$ the 10 experimental intensities of Chu et al. [29] were used to further improve the line list. The result was used to replace the HITRAN data whilst retaining previous HITRAN values for the air broadening, self-broadening, pressure shift, and temperature dependence values. This led to removal of 51 HITRAN lines which are considered unreliable. There were also 1416 lines new to HITRAN, for which, self-broadening, pressure shift, and temperature dependence data were not available. A comparison of the resulting line list and the previous HITRAN data are seen in Fig. 7. As discussed above the new intensities are seen to be approximately twice the strength of the previous HITRAN intensities. Furthermore, positions were changed significantly, in some cases by over 10 cm^{-1}.

For the $\nu_2+\nu_4-\nu_4$, $\nu_4-\nu_2$, $\nu_4-\nu_4$ and $2\nu_2-2\nu_2$ hot bands all lines stronger than the HITRAN threshold were added directly to the HITRAN data set. The numbers of new lines and band strengths for the new data are included in Table 7 alongside the total BYTe band strengths. Although this is a significant improvement to the data set, new measurements in these regions are still desirable.

9. Conclusions

A critical and careful analysis of large experimental and theoretical datasets has been carried out. Translation between the normal mode and local mode treatments is explored and the local mode labels of BYTe which are used to provide quantum numbers in the new dataset. Section 2 species a complete set of quantum labels which uniquely describes all ammonia's rovibrational energy levels; no such complete set appears to have been previous specified for this system. Whilst data belonging to HITRAN, usually being the result of Hamiltonian fits, are retained where desirable, new assignments and labelings are made using both CD's and the BYTe line list in regions where new Hamiltonian fits were either not feasible or not worthwhile.

Results indicate a total of 360 new assignments as well as a further 382 new upper labelings are obtained for the problem HITRAN lines as tabulated in Table 4. In total, 229 assignments have been made for the unassigned lines in HITRAN, and 446 new labelings found for unlabeled HITRAN lines. The remainder of the assignments constitute reassignments of HITRAN lines for which assignments were brought into question by the initial analysis. In addition to these assignments the $2\nu_2-\nu_2$ band has updated positions and intensities (including 1416 new lines), and 10 264 lines belonging to the $\nu_2+\nu_4-\nu_4$, $\nu_4-\nu_2$, $\nu_4-\nu_4$ and $2\nu_2-2\nu_2$ hot bands are included for the first time. Intensities are also updated for the ν_2 band, using 144 experimental values where available, and BYTe values elsewhere. A summary of the updated line list is given in Table 7, with tentative assignments to new vibrational bands summarized in Table 5.

The results provided in the supplement, consist of a line list of 40 227 transitions, with average upper level deviations of 7.7×10^{-4} cm^{-1} and verified quantum labels in the range 0–5300 cm^{-1}. Lines for which assignments were questioned for any of the aforementioned reasons have been included with their previous HITRAN assignments but are marked as unassigned.

In total 9979 of the HITRAN Einstein A coefficients have been altered by more than 1% in this work, since new J, Γ and lower energy values alter predictions of A values derived from the experimental intensities. The new line list includes these updated A values along with 2800 updated values for the statistical weights.

In terms of the HITRAN data we suggest the inclusion of both vibrational and total symmetry species as well as the addition of L_3 and L_4 labels to future releases of HITRAN. The new data format, XSAMS [61] and on-line services being developed by the Virtual Atomic and Molecular Data Center (VAMDC) [62] have the flexibility to describe all the necessary quantum numbers. This new HITRAN online service is now available as part of the 2012 release [63].

This analysis improves the reliability of the HITRAN dataset as a tool for assignment and identification of spectra; in particular the temperature dependence is improved by correction of lower assignments. Recently published analysis by Sung et al. [36] and Cacciani et al. [58] provide a considerable number of assignments in the 6000–6300 cm^{-1} region which should be used to further extend the HITRAN dataset.

We supply an updated and improved $^{14}NH_3$ line list in HITRAN format in the supplementary data with all assignments converted to the recommended labels of Eq. (1). A file containing our recommended experimental energy levels is also supplied for use in any future analysis of ammonia containing spectra. This work has been submitted to HITRAN for inclusion in the 2012 revision [59].

Acknowledgments

This work is supported by a the UK Natural Environmental Research Council (NERC) via a studentship to MJD, by ERC Advanced Investigator Project 267219 and the VAMDC project which is funded by the European Union INFRA-2008-1.2.2 Scientific Data Infrastructure program under Grant Agreement number 239108. Part of the research described in this paper was performed at the Jet Propulsion Laboratory, California Institute of Technology, under contracts and grants with the National Aeronautics and Space Administration.

Appendix A. Supplementary data

Supplementary data associated with this article can be found in the online version at http://dx.doi.org/10.1016/j.jqsrt.2013.05.027.

References

[1] Galloway JN, Aber JD, Erisman JW, Seitzinger SP, Howarth RW, Cowling EB, et al. The nitrogen cascade. Bioscience 2003;53:341–56.
[2] Sutton M, Reis S, Baker S, editors. Atmospheric ammonia: detecting emission changes and environmental impacts. In: Results of an expert workshop under the convention on long-range transboundary air pollution. Springer; 2009.
[3] Gruber N, Galloway JN. An Earth-system perspective of the global nitrogen cycle. Nature 2008;451:293–6.
[4] Galloway JN, Dentener FJ, Capone DG, Boyer EW, Howarth RW, Seitzinger SP, et al. Nitrogen cycles: past, present, and future. Biogeochemistry 2004;70:153–226.
[5] Clarisse L, Clerbaux C, Dentener F, Hurtmans D, Coheur PF. Global ammonia distribution derived from infrared satellite observations. Nature Geosci 2009;2:479–83.
[6] Burgess AB, Dudhia A, Grainger RG, Stevenson D. Progress in tropospheric ammonia retrieval from the MIPAS satellite instrument. Adv Space Res 2006;37:2218–21.
[7] Beer R, Shephard MW, Kulawik SS, Clough SA, Eldering A, Bowman KW, et al. First satellite observations of lower tropospheric ammonia and methanol. Geophys Res Lett 2008;35:L09801.
[8] von Bobrutzki K, Braban CF, Famulari D, Jones SK, Blackall T, Smith TEL, et al. Field inter-comparison of eleven atmospheric ammonia measurement techniques. Atmos Meas Tech 2010;3:91–112.
[9] Lara L-M, Bézard B, Griffith CA, Lacy JH, Owen T. High-resolution 10-micronmeter spectroscopy of ammonia and phosphine lines on Jupiter. Icarus 1998;131:317–33. http://dx.doi.org/10.1006/icar.1997.5868.
[10] Burrows A, Marley M, Hubbard WB, Lunine JI, Guillot T, Saumon D, et al. A nongray theory of extrasolar giant planets and brown dwarfs. Astrophys J 1997;491:856–75. http://dx.doi.org/10.1086/305002.
[11] Sharp CM, Burrows A. Atomic and molecular opacities for brown dwarf and giant planet atmospheres. Astrophys J 2007;168:140–66. http://dx.doi.org/10.1086/508708.

[12] Beaulieu JP, Tinetti G, Kipping D, Ribas I, Barber RJ, Cho JY-K, et al. Probing the atmosphere of the transiting hot Neptune GJ436b. Astrophys J 2011;731:16.

[13] Moses JI, Visscher C, Fortney JJ, Showman AP, Lewis NK, Griffith CA, et al. Disequilibrium carbon, oxygen, and nitrogen chemistry in the atmospheres of HD 189733b and HD 209458b. Astrophys J 2011;737:15. http://dx.doi.org/10.1088/0004-637X/737/1/15.

[14] Rothman LS, Gordon IE, Barbe A, Benner DC, Bernath PF, Birk M, et al. The *HITRAN*2008 molecular spectroscopic database. J Quant Spectrosc Radiat Transfer 2009;110:533–72.

[15] Rothman LS, Gamache RR, Goldman A, Brown LR, Toth RA, Picket HM, et al. The HITRAN database: 1986 edition. Appl Opt 1987;26:4058–97.

[16] Geulachvili G, Abdullah AH, Tu N, Rao KN, Urban Š, Papoušek D. Analysis of high-resolution Fourier transform spectra of $^{14}NH_3$ at 3.0 μm. J Mol Spectrosc 1989;133:345–64.

[17] Urban Š, Tu N, Rao KN, Geulachvili G. Analysis of high-resolution Fourier transform spectra of $^{14}NH_3$ at 2.3 μm. J Mol Spectrosc 1989;133:312–30.

[18] Kleiner I, Tarrago G, Brown LR. Positions and intensities in the $3\nu_2/\nu_2+\nu_4$ vibrational system of $^{14}NH_3$ near 4 micron. J Mol Spectrosc 1995;173:120–54.

[19] Brown LR, Margolis JS. Empirical line parameters of $^{14}NH_3$ from 4791 cm^{-1} to 5294 cm^{-1}. J Quant Spectrosc Radiat Transfer 1996;56:283–94.

[20] Cottaz C, Kleiner I, Tarrago G, Brown LR, Margolis JS, Poynter RL, et al. Line positions and intensities in the $2\nu_2/\nu_4$ vibrational system of $^{14}NH_3$ near 5–7 μm. J Mol Spectrosc 2000;203:285–309.

[21] Cottaz C, Tarrago G, Kleiner I, Brown LR. Assignments and intensities of $^{14}NH_3$ hot bands in the 5–8 μm ($3\nu_2-\nu_2$, $\nu_2+\nu_4-\nu_2$) and 4 μm ($4\nu_2-\nu_2$, $\nu_1-\nu_2$, $\nu_3-\nu_2$) regions. J Mol Spectrosc 2001;209:30–49.

[22] Cottaz C. 4 μm hot bands. PhD thesis. Universite de Paris-Sud; 2000.

[23] Kleiner I, Brown LR, Tarrago G, Kou Q-L, Picqué N, Geulachvili G, et al. Line positions and intensities in the $2\nu_4/\nu_1/\nu_3$ vibrational system of $^{14}NH_3$ near 3 μm. J Mol Spectrosc 1999;193:46–71.

[24] Pearson J. Rotational $\nu_2-\nu_2$ and ν_2–ground state prediction, jPL (private communication), quoted in the HITRAN reference file; 2000.

[25] Guinet M, Jeseck P, Mondelain D, Pepin I, Janssen C, Camy-Peyret C, et al. Absolute measurements of intensities, positions and self-broadening coefficients of R branch transitions in the ν_2 band of ammonia. J Quant Spectrosc Radiat Transfer 2011;112:1950–60. http://dx.doi.org/10.1016/j.jqsrt.2011.03.015.

[26] Fabian M, Yamada K. Absolute intensity of the NH_3 ν_2 band. J Mol Spectrosc 1999;198:102–9. http://dx.doi.org/10.1006/jmsp.1999.7937.

[27] Nemtchinov V, Sung K, Varanasi P. Measurements of line intensities and half-widths in the 10 μm bands of $^{14}NH_3$. J Quant Spectrosc Radiat Transfer 2004;83:243–65. http://dx.doi.org/10.1016/S0022-4073(02)00354-0.

[28] Aroui H, Nouri S, Bouanich J. NH_3 self-broadening coefficients in the ν_2 and ν_4 bands and line intensities in the ν_2 band. J Mol Spectrosc 2003;220:248–58. http://dx.doi.org/10.1016/S0022-2852(03)00124-3.

[29] Chu Z, Chen L, Cheo PK. Absorption spectra of NH_3 using a microwave-sideband CO_2-laser spectrometer. J Quant Spectrosc Radiat Transfer 1994;51:591–602. http://dx.doi.org/10.1016/0022-4073(94)90113-9.

[30] Huang X, Schwenke DW, Lee TJ. An accurate global potential energy surface, dipole moment surface and rovibrational frequencies for NH_3. J Chem Phys 2008;129:214304.

[31] Huang X, Schwenke DW, Lee TJ. Rovibrational spectra of ammonia. Part I: unprecedented accuracy of a potential energy surface used with nonadiabatic corrections. J Chem Phys 2011;134:044320.

[32] Huang X, Schwenke DW, Lee TJ. Rovibrational spectra of ammonia. Part II: detailed analysis, comparison, and prediction of spectroscopic assignments for $^{14}NH_3$, $^{15}NH_3$, and $^{14}ND_3$. J Chem Phys 2011;134:044321.

[33] Yurchenko SN, Barber RJ, Yachmenev A, Thiel W, Jensen P, Tennyson J. A variationally computed $T=300$ K line list for NH_3. J Phys Chem A 2009;113:11845–55.

[34] Yurchenko SN, Barber RJ, Tennyson J. A variationally computed hot line list for NH_3. Mon Not R Astr Soc 2011;413:1828–34.

[35] Bunker PR, Jensen P. Molecular symmetry and spectroscopy. second ed.Ottawa: NRC Research Press; 1998.

[36] Sung K, Brown LR, Huang X, Schwenke DW, Lee TJ, Coy SL, et al. Extended line positions, intensities, empirical lower state energies and quantum assignments of NH_3 from 6300 to 7000 cm^{-1}. J Quant Spectrosc Radiat Transfer 2012;113:1066–83.

[37] Yurchenko SN, Barber RJ, Tennyson J, Thiel W, Jensen P. Towards efficient refinement of molecular potential energy surfaces: ammonia as a case study. J Mol Spectrosc 2011;268:123–9.

[38] Yurchenko SN, Zheng J, Lin H, Jensen P, Thiel W. Dipole moment and rovibrational intensities in the electronic ground state of NH_3: bridging the gap between ab initio theory and spectroscopic experiment. J Chem Phys 2005;123:134308.

[39] Yurchenko SN, Thiel W, Jensen P. Theoretical rovibrational energies (TROVE): a robust numerical approach to the calculation of rovibrational energies for polyatomic molecules. J Mol Spectrosc 2007;245(2):126–40.

[40] Lynas-Gray AE, Miller S, Tennyson J. Infra red transition intensities for water: a comparison of *ab initio* and fitted dipole moment surfaces. J Mol Spectrosc 1995;169:458–67.

[41] Lodi L, Tennyson J, Polyansky OL. A global, high accuracy ab initio dipole moment surface for the electronic ground state of the water molecule. J Chem Phys 2011;135:034113.

[42] Herzberg G. Infrared and raman spectra of polyatomic molecules. D. Van Nostrand Company Inc.; 1945.

[43] Yurchenko SN, Carvajal M, Jensen P, Lin H, Zheng J, Thiel W. Rotation–vibration motion of pyramidal XY_3 molecules described in the Eckart frame: theory and application to NH_3. Mol Phys 2005;103:359–78.

[44] Hougen J. Classification of rotational energy levels for symmetric-top molecules. J Chem Phys 1962;37:1433–44. http://dx.doi.org/10.1063/1.1733301.

[45] Urban Š, Špirko V, Papoušek D, McDowell RS, Nereson NG, Belov SP, et al. Coriolis and l-type interactions in the ν_2, $2\nu_2$, and ν_4 states of $^{14}NH_3$. J Mol Spectrosc 1980;79:455–95. http://dx.doi.org/10.1016/0022-2852(80)90226-X.

[46] Urban Š. Effective rotational Hamiltonians of pyramidal XY_3 molecules with the inversion splittings of energy levels. J Mol Spectrosc 1988;131:133–53. http://dx.doi.org/10.1016/0022-2852(88)90113-0.

[47] Špirko V, Stone JMR, Papoušek D. Vibration–inversion–rotation spectra of ammonia: centrifugal distortion, Coriolis interactions, and force field in $^{14}NH_3$, $^{15}NH_3$, $^{14}ND_3$, and $^{14}NT_3$. J Mol Spectrosc 1976;60:159–78. http://dx.doi.org/10.1016/0022-2852(76)90123-5.

[48] Boudon V, Rey M, Loëte M. The vibrational levels of methane obtained from analyses of high-resolution spectra. J Quant Spectrosc Radiat Transfer 2006;98(3):394–404. http://dx.doi.org/10.1016/j.jqsrt.2005.06.003.

[49] Watson JKG. Higher-order vibration–rotation energies of the X_3 molecule. J Mol Spectrosc 1984;103:350–63. http://dx.doi.org/10.1016/0022-2852(84)90062-6.

[50] Lindsay C, McCall BJ. Comprehensive evaluation and compilation of H_3^+ spectroscopy. J Mol Spectrosc 2001;210:60–83. http://dx.doi.org/10.1006/jmsp.2001.8444.

[51] Ouardi O, Hilico JC, Loete M, Brown LR. The hot bands of methane between 5 and 10 μm. J Mol Spectrosc 1996;180:311–22, http://dx.doi.org/10.1006/jmsp.1996.0254.

[52] Kleiner I, Tarrago G, Cottaz C, Sagui L, Brown LR, Poynter RL, et al. NH_3 and PH_3 line parameters: the 2000 HITRAN update and new results. J Quant Spectrosc Radiat Transfer 2003;82:293–312.

[53] Chen P, Pearson JC, Picket HM, Matsuura S, Blake GA. Measurements of $^{14}NH_3$ in the $\nu_2=1$ state by a solid state, photo-mixing, THz spectrometer, and a simultaneous analysis of the microwave, terahertz, and infrared transitions between the ground and ν_2 inversion–rotation levels. J Mol Spectrosc 2006;236:116–26.

[54] Yu S, Pearson J, Drouin B, Sung K, Pirali O, Vervloet M, et al. Submillimeter-wave and far-infrared spectroscopy of high-J transitions of the ground and $\nu_2=1$ states of ammonia. J Chem Phys 2010;137:174317.

[55] Polyansky OL, Zobov NF, Viti S, Tennyson J, Bernath PF, Wallace L. K band spectrum of water in sunspots. Astrophys J 1997;489:L205–8.

[56] Lodi L, Tennyson J. Line lists for $H_2{}^{18}O$ and $H_2{}^{17}O$ based on empirically-adjusted line positions and ab initio intensities. J Quant Spectrosc Radiat Transfer 2012;113:850–8.

[57] Owen K, Et-touhami Es-sebbar S, Aamir Farooq S. Measurements of NH_3 line strengths and collisional broadening coefficients in N_2, O_2, CO_2, and H_2O near 1103.46 cm^1. J Quant Spectrosc Radiat Transfer 2013;121(0):56–68. http://dx.doi.org/10.1016/j.jqsrt.2013.02.001.

[58] Cacciani P, Cermak P, Cosleou J, Khelkhal M, Jeseck P, Michaut X. New progress in spectroscopy of ammonia in the infrared range using evolution of spectra from 300 K down to 122 K. J Quant Spectrosc Radiat Transfer 2012;113:1084–91. http://dx.doi.org/10.1016/j.jqsrt.2012.02.026.

[59] Rothman LS, Gordon IE, Babikov Y, Barbe A, Benner DC, Bernath PF et al. The HITRAN database: 2012 edition. J Quant Spectrosc Radiat Transfer.

[60] Rothman LS, Jacquemart D, Barbe A, Benner DC, Birk M, Brown LR, et al. The *HITRAN*2004 molecular spectroscopic database. J Quant Spectrosc Radiat Transfer 2005;96:139–204.
[61] Dubernet M, Humbert D, Ralchenko Y, Roueff E, Schultz D, Chung H, et al. XSAMS: XML schema for atomic, molecular and solid data ⟨http://www-amdis.iaea.org/xsams/docu/xsams-0.1.1.pdf⟩ (2011).
[62] Dubernet ML, Boudon V, Culhane JL, Dimitrijevic MS, Fazliev AZ, Joblin C, et al. Virtual atomic and molecular data centre. J Quant Spectrosc Radiat Transfer 2010;111:2151–9.
[63] Hill C, Gordon IE, Rothman LS, Tennyson J. A new relational database structure and online interface for the HITRAN database. J Quant Spectrosc Radiat Transfer. http://dx.doi.org/10.1016/j.jqsrt.2013.04.027.